J Electr Eng Technol.2018; 13(3): 1317-1325
http://doi.org/10.5370/JEET.2018.13.3.1317

ISSN(Print) 1975-0102
ISSN(Online) 2093-7423

Study on Leading-phase Operation Capability of a 770 MW Jumbo Hydro-generator based on Stability Analysis and End-Region Heat Analysis

Zhen-nan Fan†, Zhi-ting Zhou*, Jian-fu Li, Kun Wen*, Jun Wang*, Zhang Sun*, Tao Wang* and Bing Yao***

Abstract – A generator-grid coupling calculation model is established to study the leading-phase operational capability of a 770 MW jumbo hydro-generator in a Chinese ultra-mega hydropower station. The static and dynamic stability of the generator are analyzed and calculated to obtain stability limits under leading-phase operating conditions. Three-dimensional (3D) time-varying nonlinear moving electromagnetic and temperature field models of the generator end-region are also established and used to determine the magnetic field, loss, and temperature of the end-region under the leading-phase operating condition. The simulation results agree with data measured from the actual 770 MW hydro-generator. This paper provides reliable reference data for the leading-phase operation of a jumbo hydro-generator, which will help to improve in the design and manufacture of future hydro-generators.

Keywords: 770MW jumbo hydroelectric generator, Leading-phase operation capability, Power system stability, Electromagnetic analysis, Temperature.

1. Introduction

The rapid development of the power system has been accompanied by increases in high voltage transmission capacities and distances, which in turn has led to a significant increase in grid charging reactive power. This condition often means that excess voltage is generated in some grid regions, which can have adverse effects on the operating safety and stability of power equipment. Traditional methods for absorbing excess reactive power such as the installation of shunt reactors or compensators require large equipment investments and do not achieve smooth adjustment, making it difficult for such systems to meet power system stability and safety requirements.

A large generator operating under a leading-phase condition, can effectively reduce the excess reactive power of the system without the need to increase auxiliary equipment or find additional power loads, which can economically and simply improve the power quality of the system. In the current Chinese power system, in which many ultra-mega hydro-generators such as the Three Gorges and Xiangjiaba installations have been added to the grid in recent years, the equipment has already been provided to enable this mode of operation for the regulation of excess reactive power. However, the effectiveness of absorbing reactive power by a large-scale generator operating under leading-phase conditions is constrained by several key factors: the static and dynamic stability limit of generator operation; the heat degree of the stator end-region components; and the lowest limit of the service power voltage. To determine the static and dynamic operating stability limit of a generator's leading-phase operating characteristics and maximize the leading-phase performance, it is necessary to carry out comprehensive, in-depth, and accurate analysis and calculate its operational stability and end-region component heating profile under leading-phase conditions. Although such circuit and field analyses have previously been used to produce worthwhile results pertaining to electrical machine operating characteristics [1-13], prior to this study there has been no characterization or site testing of the stability limits or end-region heating of a 770 MW jumbo hydro-generator.

To address this gap, this paper presents an analysis based on a generator-grid coupling calculation model of the static and dynamic stability limits of the leading-phase condition of a real 770 MW jumbo hydro-generator installed in an ultra-mega hydropower station. Three-dimensional (3D) modeling of the magnetic flux density and temperature of the generator end-region under the leading-phase condition is carried out through the application of a 3D time-varying nonlinear moving electromagnetic field model and a 3D temperature field model. Through these calculations, the performance data of the leading-phase operating condition of the hydro-generator are obtained, and the results are verified through site testing.

† Corresponding Author: The Key Laboratory of Fluid and Power Machinery, Ministry of Education, Xihua University, Chengdu China. (fanzhennan@126.com)
* The Key Laboratory of Fluid and Power Machinery, Ministry of Education, Xihua University, Chengdu, China. ({dianyingcc, wkk_xhu, wangjun_xhu, yaob_xhu@126.com}, {383623076,736678662}@qq.com)
** Dong Fang Electrical Machinery Co., Ltd., Deyang, China. (zouhui_a@126.com)
Received: October 6,2017; Accepted: January 26,2018

Copyright ⓒ The Korean Institute of Electrical Engineers
This is an Open-Access article distributed under the terms of the Creative Commons Attribution Non-Commercial License (http://creativecommons.org/licenses/by-nc/3.0/) which permits unrestricted non-commercial use, distribution, and reproduction in any medium, provided the original work is properly cited.

2. Calculation Models

2.1 The basic condition of the hydro-generator

The hydropower station is located in China's Jinsha River Valley. Construction took a total of 13 years, starting in August 2003 and ending in 2015. The power plant is sited underground to the left and right sides of the mountain body and comprises 18 jumbo 770 MW hydro-generators, as shown in Fig. 1. Basic per-generator data are listed in Table 1.

2.2 Generator - grid coupling simulation model

The generator-grid coupling model was developed using the SIMSEN software package [14]. By calculating and comparing the stability of different leading-phase operating points, the limit operating point of the generator was calculated to represent the depth of leading phase operation. The model comprises components including a generator, transformers, transmission lines, a hydro-turbine, and an infinite bus and is sub-divided into a power grid, electrical machinery, and a mechanical system. The grid comprises a voltage source equivalent to the infinite bus and an R-L-C loop equivalent to the transmission line and transformer. The mechanical system comprises two concentrated mass modules, the generator rotor, and the hydro-turbine. To better reflect the actual operational conditions of the generator and make the calculation more accurate, the excitation and speed control systems and the impact of the generator magnetic circuit saturation are also considered. A model wiring diagram of the assembly is shown in Fig. 2.

The symbols in Fig. 2 are defined in Table 2.

(a) Power station panorama

(b) 770 MW jumbo hydro-generators

Fig. 1. Photographs of power station and generators

Table 1. Basic data of the generator

Parameter	Value
Rated Capacity (MVA)	855.6
Rated power (MW)	770
Rated voltage (kV)	20
Rated current (A)	24,698
Power factor	0.9
Rated speed (r/min)	125
Rated excitation current (A)	3530
Direct - axis transient reactance X_d/p.u.	0.9085
Cross - axis synchronous reactance X_q/p.u.	0.6649
Direct - axis transient reactance X_d' /p.u.	0.3259
Cross - axis transient reactance X_q'/p.u.	0.6649
Direct - axis transient reactance X_d'' /p.u.	0.2414
Cross - axis transient reactance X_q''/p.u.	0.2604

Table 2. Fig. 2 symbol definitions

Symbol	Meaning
VSN	Voltage Supply
VSN-1	Neutral Terminal
GND-2	RLC Impedance
LN1	Transmission Line 1
CB	Circuit Breaker
LN	Transmission Line
TN	Transformer
TN-1	Neutral Terminal
GND1	RLC Impedance 1
CBN	Circuit Breaker
VMF	Low-Pass Filter
TEX	Transformer
VERG	Regulator
SM	Synchronous Machine
ME1	Mechanical Mass 1
ME2	Mechanical Mass 2
CBEX1	Single Phase Circuit Breaker 1
ICONVEX	Current Converter
ARCCOS	Program
CBEX1	Single Phase Circuit Breaker 2
REX	Single Phase RLC Impedance
SAT	Saturation
TORQUE	Points Function of Active Power
Q	Points Function of Reactive Power

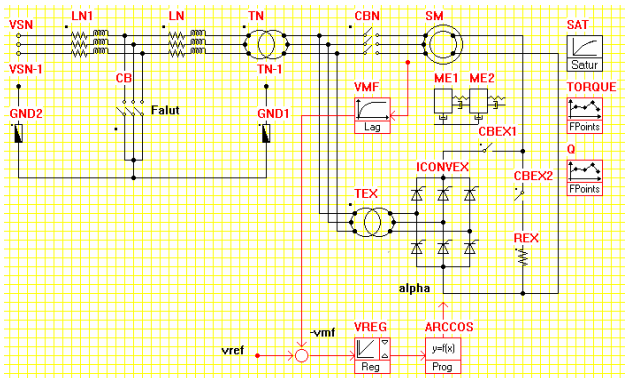

Fig. 2. Wiring diagram of the generator-grid coupling model

2.3 3D time-varying nonlinear moving electromagnetic field model

Based on consideration of factors such as core saturation, conductor eddy current, rotor rotation, and the 3D structure of the end winding, a 3D time-varying nonlinear moving electromagnetic field model was established to analyze the eddy current loss of the hydrogenerator end-region components under the leading-phase operating condition.

Based on the periodicity of the magnetic field, a pair of poles at the end region were chosen as the 3D electromagnetic field calculation region, as shown in Fig. 3.

Assuming core saturation, the coulomb norm $\nabla \cdot A = 0$ and the boundary condition of the problem region can be applied to obtain the 3D boundary value problem of the nonlinear time-varying moving electromagnetic field as follows:

$$\begin{cases} \nabla \times (\nu \nabla \times \mathbf{A}) + \dfrac{1}{\rho}\left[\dfrac{\partial \mathbf{A}}{\partial t} - \mathbf{V} \times (\nabla \times \mathbf{A})\right] = \mathbf{J}_S \\ \left.\begin{aligned} \mathbf{n} \times \mathbf{A} &= 0 \\ \dfrac{\partial A_n}{\partial n} &= 0 \end{aligned}\right\} S_1, S_2, S_3 \\ \mathbf{A}\big|_{S_4} = \mathbf{A}\big|_{S_5} \end{cases} \tag{1}$$

where A_n is the normal component of $\boldsymbol{A}$, S_1 is the symmetric boundary surface parallel to the flux line, S_2 is the end shade, S3 is the end cover idealized boundary with $\rho = 0$ containing only the tangential components of the magnetic field, and S_4 and S_5 are periodic boundary surfaces that meet the cyclic boundary condition.

Time-step computation of the 3D moving electromagnetic field model of the end-region are used to obtain the flux density, eddy current, and iron losses. These three losses are then used as heat sources in the 3D-temperature field calculation of the generator end-region.

2.4 Boundary value problem of end-region 3D temperature field

The solving region for the 3D temperature field is the stator end-region, including the clamping plate, pressure finger, end-region ladder core, etc., as shown in Fig. 4. Assuming anisotropic heat conduction in the laminated core, the boundary value problem of the 3D steady temperature field can be expressed as follows:

$$\begin{cases} \dfrac{\partial}{\partial x}(\lambda_x \dfrac{\partial T}{\partial x}) + \dfrac{\partial}{\partial y}(\lambda_y \dfrac{\partial T}{\partial y}) + \dfrac{\partial}{\partial z}(\lambda_z \dfrac{\partial T}{\partial z}) = -q_V \\ \lambda \dfrac{\partial T}{\partial n}\Big|_S = -\alpha(T - T_f) \end{cases} \tag{2}$$

Where T is temperature, λ_x, λ_y, and λ_z are the coefficients of thermal conductivity in different directions, and q_v is the heat source density, which is obtained from the previous 3D time-varying nonlinear moving electromagnetic field calculation.

The indices S in Eq. (2) correspond to the surfaces of the stator end region related to the heat dissipation boundary condition; α is the heat transfer coefficient on S, and T_f is the environmental temperature.

3. Stability Calculation Results and Discussions

3.1 Stability computation model validation

To verify the accuracy and suitability of the above generator-grid coupling model, we introduce here the leading-phase operating depth test based on the Chinese National Standard Q/GDW 746-2012 Synchronous Generator Leading-Phase Test Guideline [15]. In this test, active power, reactive power, stator voltage, stator current, power-angle, system voltage, service power voltage, and other excitation parameters are measured and compared

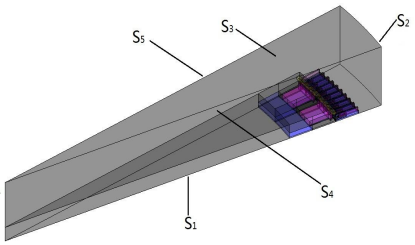

(a) Problem region for 3D moving electromagnetic field computation

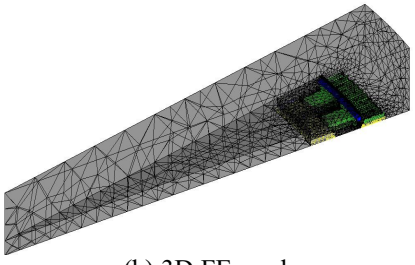

(b) 3D FE meshes

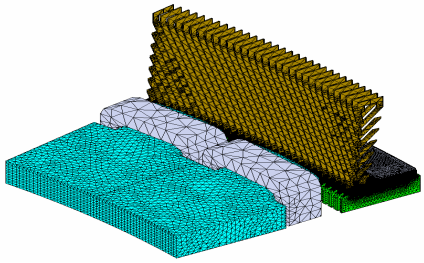

(c) FE mesh detail

Fig. 3. Problem region and FM meshes used for 3D electromagnetic field calculation

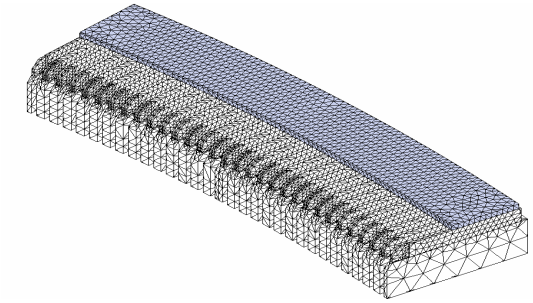

Fig. 4. The Problem region and FM meshes of 3D temperature field calculation

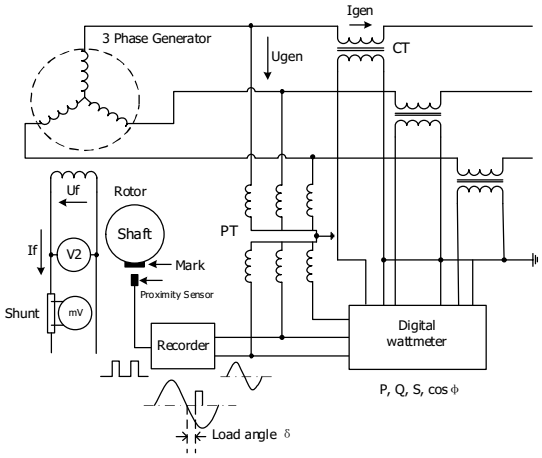

(a) Leading-phase test schematic circuit

(b) Test site and instrument

Fig. 5. Leading-phase test

with calculated values. The measurement circuit that was applied in conducting this test to the generator and grid system is shown in Fig. 5.

To ensure the safety of the generator and grid, the test conditions had to meet the following requirements of the Chinese National Standard Q/GDW 746-2012 Synchronous Generator Leading-Phase Test Guideline [15]. First, the generator stator current could not exceed the rated value (24,697.6 A). Second, the generator stator voltage could not be lower than 90% of the rated value (18 kV). Third, the temperature of the stator core end-region and its pressure finger could not be higher than 120℃, while the temperature of the clamping plate could not exceed 200℃. Fourth, the service power voltage could not be less than 93% of the rated value, that is, it could not be less than

Table 3. Comparison of calculated and test values of generator power-angle

Active power (MW)	Reactive power (MVar)	Power-angle (°)		Error (%)
		Calculate value	Test value	
2.5	−296.9			
459.4	−310.0	32.4	31.8	−1.8
572.2	−314.1	38.2	39.1	2.3
697.1	−251.0	41.0	42.2	2.9
764.9	−233.0	42.1	43.2	2.6

Table 4. Other generator and hydroelectric power station electrical parameter test values

Active power (MW)	Reactive power (MVar)	Power factor	Stator voltage (kV)	Stator current (kA)	Bus voltage (kV)	Service power voltage (kV)
2.5	−296.9	0.008	18.7	9.2	533.4	9.7
459.4	−310.0	0.829	18.6	17.4	533.7	9.9
572.2	−314.1	0.877	18.6	20.5	535.4	9.7*
697.1	−251.0	0.941	18.7	22.9	533.7	9.9
764.9	−233.0	0.957	18.8	24.8	535.5	9.9

Table 5. Calculated generator leading-phase conditions

Parameter	Operating points of generator							
	1	2	3*	4	5	6	7	8*
P (MW)	770	770	770	770	770	770	770	770
Q (MVar)	372.9	0	−372.9	−500	−600	−700	−800	−868.5
U_s (kV)	21.4	21.44	20.27	19.88	19.57	19.26	18.94	18.73
δ (°)	22.478	27.847	38.717	43.821	48.471	53.729	59.605	63.969
$cos\varphi$	0.9	1	−0.9	−0.839	−0.789	−0.74	−0.693	−0.663
δ_{max} (°)	50.076	53.754	57.293	58.647	59.828	61.167	62.737	63.989
I_s (kA)	23.08	20.74	24.36	26.67	28.8	31.2	33.84	35.78

9.765 kV. Fifth, the system voltage (500 kV) could not be less than the lower limit of the operating voltage curve given by the power dispatching department (534 kV). In addition, in carrying out the test, a certain margin of stability was required and the field-loss protection action of the generator had to be prevented.

Some of the calculation and test results are shown in Tables 3 and 4, which indicate that the test data are in good agreement with the calculation values. Based on this, it can be concluded that the generator-grid coupling model is accurate and suitable for solving the stability limit of the generator leading-phase operating condition.

3.2 Static stability limit analysis

In the simulation calculations, the active power remained stable at 770 MW and the reactive power was regulated after entering the leading-phase operation condition through a reduction from the rated operating point of 372.9 MVar (power factor 0.9) down to the static stability limit point. The simulation results of this regulation are shown in Fig. 6 and Table 5.

In Table 5, P is the active power, Q is the reactive power, U_s is the stator voltage, δ is the power-angle, cosφ is the power factor, δ_{max} is the maximum power factor, and I_s is

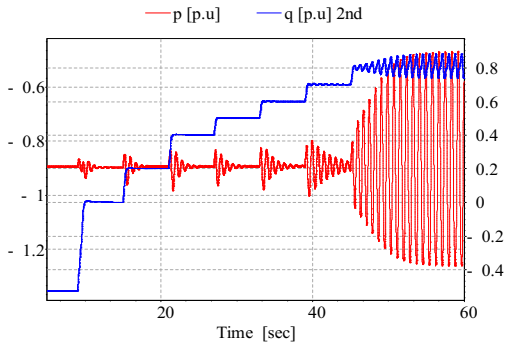

(a) Active and reactive power

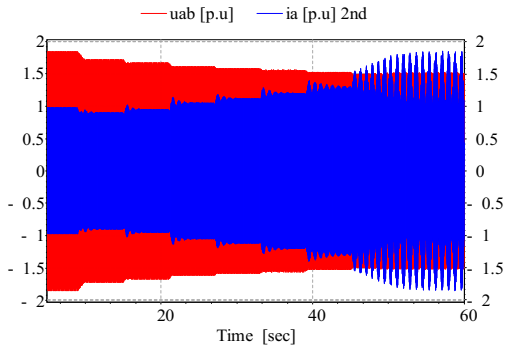

(b) Stator voltage and current

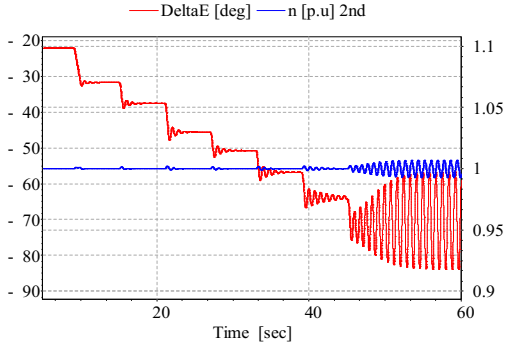

(c) Power angle and speed

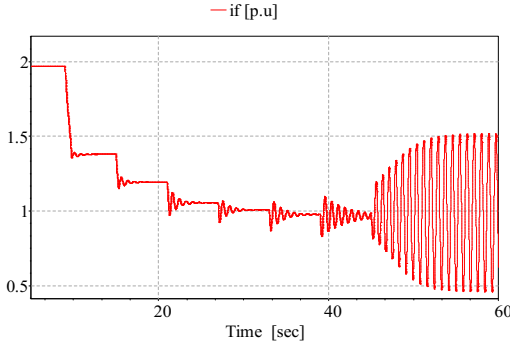

(d) Excitation current

Fig. 6 Static stability limit simulation results

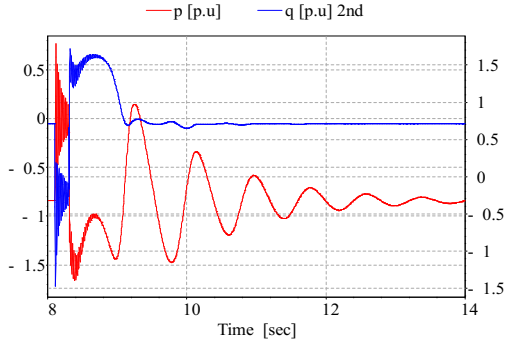

(a) Active and reactive power curves

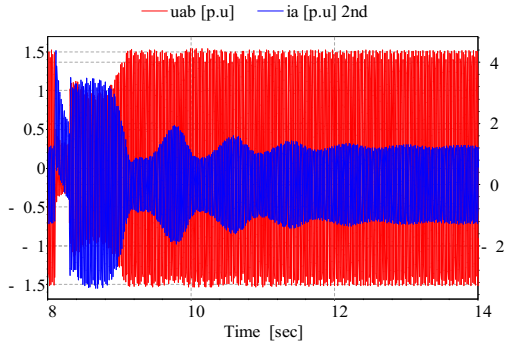

(b) Generator stator voltage and stator current curves

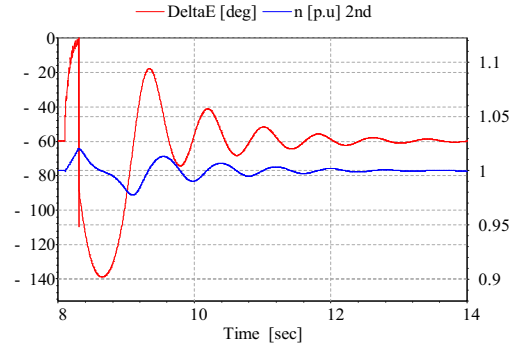

(c) Generator power-angle and speed curve

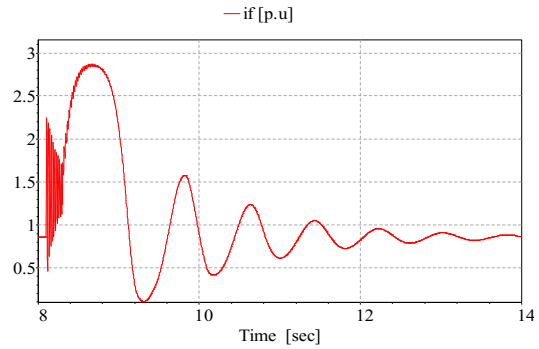

(d) Excitation current curve

Fig. 7. Dynamic stability simulation results (P = 770 MW, Q = -477 MVar)

the stator current.

From the above figures and table, it is seen that reducing current and stator voltage while gradually increasing the stator current and power-angle. Each adjustment of reactive power causes the above parameters to fluctuate and quickly restore until the leading-phase condition, in which the active and reactive power have reached 770 MW and

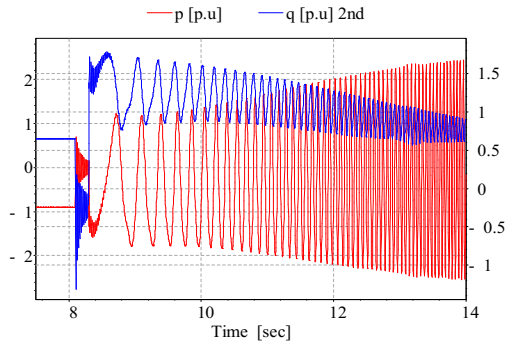

(a) Active and reactive power curves

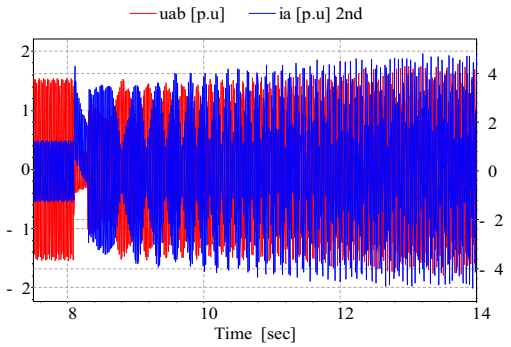

(b) Generator stator voltage and stator current curves

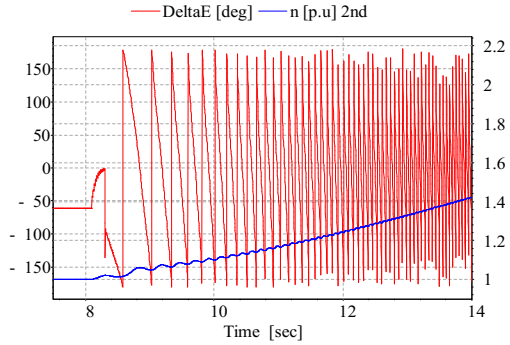

(c) Generator power-angle and speed curve

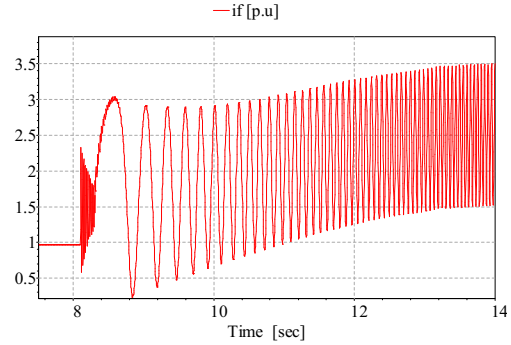

(d) Excitation current curve

Fig. 8. Dynamic stability simulation results (P = 770 MW, Q = -478 MVar)

−868.5 MVar, respectively. This state, corresponding to the eighth generator operating point in Table 5, can be considered to be the static stability limit of the generator.

However, the stator current data in this table show that, considering the generator's rated stator over-current limit of 24,698 A in actual operation, the leading-phase depth of the generator can only reach P = 770 MW, Q = −372. 9 Mvar, which is shown as the third operating point in Table 5.

3.2 Dynamic stability limit analysis

The generator-grid coupling model was then used to obtain the dynamic stability limit of the generator by simulating a sudden three-phase short-circuit fault, a condition representing the greatest threat to the dynamic stability of the power system.

In the simulation process, the generator active power remained stable at 770 MW while the reactive power was reduced from zero by 1 MW per leading-phase operating point. Each operating point simulation lasted 20 s, during which time a sudden three-phase short circuit was applied at t = 8 s and then removed after 0.6 s.

At −477 Mvar, the generator was still able to recover and maintain synchronous running even though the post-short-circuit generator power, voltage, current, power-angle, and speed all had significant oscillation amplitudes (Fig. 7); however, at the next operating point (−478 Mvar), the generator failed to resume synchronous operation after the short-circuit fault was applied and finally fell out of step.

This suggests that the dynamic stability limit of the generator was reached P = 770 MW, Q = −477 MVar, as shown in Fig. 8.

4. Calculation Results and Discussions of End-region Heat

4.1 Heat calculation model validation

To validate the accuracy and suitability of the end-region loss and heat calculation model used in this paper, the temperatures of the generator end-region components were measured following the Chinese National Standard Q/GDW 746-2012 Synchronous Generator Leading-Phase Test Guideline [15]. In the test, 10 thermocouple groups were firmly mounted on the surfaces of the end-region stator core, pressure fingers, and clamping plate with 91 fast-drying adhesive pieces. The thermocouple locations are shown in Fig. 9(a), the workflow of the temperature measuring device is shown in Fig. 9(b), the basic data of thermocouple are shown in Table 6.

Some of the test and calculation results are shown in Tables 7 to 8. Overall, the results show close agreements between the calculated and measured values, and it can be concluded that the end-region loss and heat calculation model used in this paper is accurate and suitable for analysis of heat conditions in the generator end-region.

(a) Locations of thermocouples

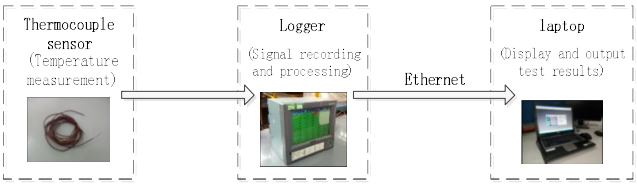

(b) The workflow of the temperature measuring device

Fig. 9. The temperature test of end region

Table 6. The basic data of thermocouple

Parameter of Thermocouple	Value
Graduation	T
Accuray class	II
Measuring range (℃)	0~419.527

Table 7. End-region stator core temperature calculated results and test data (from test points)

Active power (MW)	Reactive power (MVar)	End stator core test point temperature (℃)		Error (%)
		Calculate value	Test value	
459.4	−310.0	44.6	46.2	3.6
572.2	−314.1	46.9	48.8	4.1
697.1	−251.0	49.5	52.1	5.3
764.9	−233.0	52.8	55.2	4.5

Table 8. End-region pressure finger temperature calculated results and test data (from test points)

Active power (MW)	Reactive power (MVar)	Pressure finger test point temperature (℃)		Error (%)
		Calculated value	Test value	
459.4	−310.0	45.6	48.1	5.5
572.2	−314.1	47.2	50.1	6.1
697.1	−251.0	49.2	51.2	4.1
764.9	−233.0	50.2	53.3	6.2

Table 9. End-region pressure plate temperature calculated results and test data (from test points)

Active power (MW)	Reactive power (MVar)	Pressure plate test point temperature (℃)		Error (%)
		Calculated value	Test value	
459.4	−310.0	50.6	53.5	5.7
572.2	−314.1	54.1	55.7	3.0
697.1	−251.0	57.2	58.5	2.3
764.9	−233.0	60.1	62.2	3.5

4.2 Heat calculation of the static stability limit point of leading-phase condition

Using the above models, the magnetic field and temperature distribution of the end-region under the static stability limit point of the leading-phase condition (P = 770 MW, Q = −372.9 MVar) were calculated. Some of the results are shown in Fig. 10 and in Table 10.

The results of this calculation reveal low end-region temperatures under the leading-phase operating condition and no possibility of overheating. This is the result of a series of optimization measures taken during the electro-magnetic design phase of the generator to improve running capability, including: improving the stator and rotor core length matching, optimizing the stator coil end cone angle, and other methods to weaken the end leakage magnetic field; precisely optimizing the stator end-region core ladder structure to reduce eddy current loss; and optimizing the end-region ventilation structure to restrain the heat.

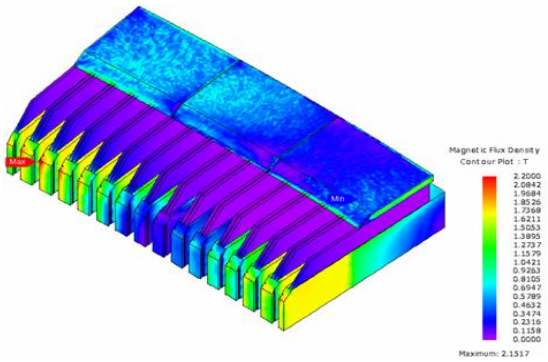

(a) The flux density

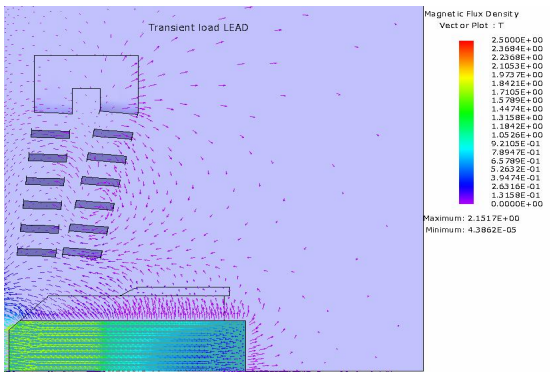

(b) The magnetic field vector

Fig. 10. Magnetic field distribution of the end-region under the static stability limit point of the leading-phase condition

Table 10. Environmental temperature values

Active power (MW)	Reactive power (MVar)	Maximum temperature (℃)		
		End-region stator core	Pressure finger	Pressure plate
770	−372.9	59.6	58.15	66.9

It is particularly noteworthy that the calculated values are in close agreement with the measured values, demonstrating that the calculation model can take the influence of a series of important factors including grid operation, generator structure, rotor rotation, magnetic saturation, etc., into account. Because the model can accurately calculate and analyze the leading-phase condition of a large hydro-generator, this method is not only useful in the analysis of the 770 MW hydro-generator analyzed paper but can be further applied to the optimization design of Chinese 1000 MW jumbo hydro-generators.

5. Conclusion

In this study, a generator-grid coupling calculation model of a real 770 MW jumbo hydro-generator was established. The static and dynamic stability of the generator were analyzed and calculated and the operating limits under the leading-phase conditions were further obtained. Two 3D field models — a time-varying nonlinear moving electromagnetic field model and a temperature field model — were established to calculate the magnetic field loss and temperature of the end-region under the leading-phase operating conditions of the generator.

The accuracy and suitability of these models were verified through direct comparisons with measured data. In addition to providing reliable reference data for the leading-phase operation of a jumbo hydro-generator, the results of this paper will help to improve the design and manufacture of this type of hydro-generator.

The research method developed in this paper has proven useful in the analysis of the leading-phase operation of real 770 MW hydro-generator; and it was used in the optimization design of the1,000 MW hydro-generators of the Baihetan hydropower Station in China.

Acknowledgements

This work was sponsored by the National natural sciences fund youth fund of China, No. 51607146 and 61703345, and the Key Scientific Research fund project of Xihua University, No.Z1520907 and Z1520909, and the Key Research fund projects of Si chuan Provincial Education Department, No. 16ZA0155 and 16ZB0159. And this work was supported by Sichuan Science and Technology Program, No. 18ZDYF3488, and this work was supported by a grant from Chunhui Project Foundation of the Education Department of China, No. Z2016144. And it was sponsored by The Key Laboratory of Fluid and Power Machinery, Ministry of Education, Xihua university, Chengdu 610039, China.

References

[1] Y. Wei, C. Jun, S. Quan-rong, "Discussion on large non-salient pole generator phase-advancement operation," *Autom. Electr. Power Syst.*, vol. 31, no. 2, pp. 94-97, 2013.

[2] X. Hai-xia, Y. Ying-ying, X. Su-ming, "Magnetic thermal coupling analysis of end region of 1000MW turbine generator," in *Proc. CSEE*, 2008, pp. 118-122.

[3] S. Jia-yan, S. Yuan-su, Z. Xiao-min, "The new method of determining the capability of leading phase of generator and realizing the no-line monitoring," in *Proc CSEE*, vol. 26, no. 11, pp. 139-143, 2006.

[4] S. Keller, M. Tu. Xuan, J. -J. Simond, and A. Chwery, "Large low-speed hydro-generator-unbalanced magnetic pulls and additional damper losses in eccentricity conditions," *IET Electr. Power Appl.*, vol. 21, no. 5, pp. 657-664, Sept. 2007.

[5] LIU Xiangyu, HE Yuling, ZHOU Wen, LIU Qingquan, CHANG Yongliang, MENG Fanchao, "Analysis on Unit Capability of Leading-phase Operation Considering Stability Restriction of Power Grid", *Journal of North China Electric Power University*, vol. 44, no. 1, pp. 52-57, 2017.

[6] Keranen, J., Ponomarev, P., Pippuri, J., et al, "Parallel Performance of Multi-Slice Finite-Element Modeling of Skewed Electrical Machines", *IEEE Trans on Magnetics*, vol. 53, no. 6, pp. 1204-1207, 2017.

[7] Huangfu, Y., Wang, S., Qiu, J., Zhang, H., et al, "Transient Performance Analysis of Induction Motor Using Field-Circuit Coupled Finite-Element Method", *IEEE Trans on Magnetics*, vol. 50, no. 2, pp. 2283-2286, 2014.

[8] Sarikhani, A., Nejadpak, A., Mohammed, O. A, "Coupled Field-Circuit Estimation of Operational Inductance in PM Synchronous Machines by a Real-Time Physics-Based Inductance Observer", *IEEE Trans. on Magnetics*, vol. 49, no. 5, pp. 2283-2286, 2013.

[9] G. Traxler-Samek, S. Lugand, and A. Schwery, "Add loss in the damper winding of large hydrogenerator at open-circuit and load conditions," *IEEE Trans. Ind. Electron.*, vol. 57, no. 1, pp. 154-160, Jan. 2010.

[10] W. Li, Y. Zhang, Y. Chen, "Calculation and analysis of heat transfer coefficients and temperature fields of air-cooled large hydro-generator rotor excitation windings," *IEEE Trans. Energy Conver.*, vol. 26, no. 3, pp. 946-952, Sept. 2011.

[11] W. Li, C. Guan, and Y. Chen, "Influence of rotation on rotor fluid and temperature distribution in a large air-cooled hydrogenerator," *IEEE Trans Energy Conver.*, vol. 28, no. 1, pp. 117-124, 2013.

[12] Z.-N. Fan, Y. Liao, L. Han, L.-D. Xie, "No-load voltage waveform optimization and damper bars heat

reduction of tubular hydro-generator by different degree of adjusting damper bar pitch and skewing stator slot, " *IEEE Trans. Energy Conver.*, vol. 28, no. 3, pp. 461-469, Sept. 2013.
[13] M.-Q. Hu and X.-L. Huang, *Numerical computation method and its application of electric machine performance.* Nanjing: Southeast University Press, 2003, 16-30.
[14] SIMSEN 2.3: Modular simulation software for the analysis of energy conversion systems, 2008.
[15] C. Hui. *Q/GDW 746-2012: Chinese national standard synchronous generator leading-phase test guideline*. Beijing: Standards Press of China, 2012.

Zhen-nan Fan He was born in Longchang, China in 1981. He received his Ph.D. degree in electrical engineering from Chongqing University, Chongqing, China, in 2013. He is currently an associate professor at Xihua University. His research interests include magnetic and thermal field calculation of generators, electrical machinery, and motor drives.

Zhi-ting Zhou She was born in Deyang, China in 1999. She is currently pursuing the B.Eng. degree at Xihua University. Her research interests include magnetic and thermal field calculation of generators, electrical machinery, and motor drives.

Jian-fu Li He received the M.Sc. degree from Huazhong University of Science and Technology University, Wuhan, China, in 2007. He is currently a senior engineer at Dong Fang Electrical Machinery Co., Ltd. His research interests include magnetic and thermal field calculation of generators, electrical machinery, and motor drives.

Kun Wen He was born in Chongqing, China in 1991. He is currently pursuing the M.Sc. degree at Xihua University. His research interests include magnetic and thermal field calculation of generators, electrical machinery, and motor drives.

Jun Wang She was born in Mianyang, China in 1966. She received the Ph.D. degree in electrical engineering from Southwest Jiaotong University, Chengdu, China, in 2006. She is currently a professor at Xihua University. Her research interests include magnetic and thermal field calculation of generators, electrical machinery, and motor drives.

Zhang Sun He was born in Lichuan, China in 1986. He received his M.Sc. degree from Xihua University, Chengdu, China, in 2013. Currently, he is a lecturer at Xihua University. His research interests include magnetic and thermal field calculation of generators, electrical machinery, and motor drives.

Tao Wang She was born in Chengdu, China, in 1986. She received the Ph.D. degree in electrical engineerin from Southwest Jiaotong University, Chengdu, China, in 2016. She is currently a lecturer at Xihua University. Her research interests include magnetic and thermal field calculation of generators, electrical machinery, and motor drives.

Bing Yao He was born in Sichuan, China in 1981. He received the M.Sc. degree Xihua University, Chengdu, China, in 2010. He is currently a lecturer at Xihua University. His research interests include magnetic and thermal field calculation of generators, electrical machinery, and motor drives.